Title
Vehicle Lateral Control Under Fault in Front and/or Rear Sensors

Authors
Lu, Guang
Huang, Jihua
Tomizuka, Masayoshi

Publication Date
2003-08-01

CALIFORNIA PATH PROGRAM
INSTITUTE OF TRANSPORTATION STUDIES
UNIVERSITY OF CALIFORNIA, BERKELEY

Vehicle Lateral Control Under Fault in Front and/or Rear Sensors

Guang Lu, Jihua Huang, Masayoshi Tomizuka
University of California, Berkeley

California PATH Research Report
UCB-ITS-PRR-2003-26

This work was performed as part of the California PATH Program of the University of California, in cooperation with the State of California Business, Transportation, and Housing Agency, Department of Transportation; and the United States Department of Transportation, Federal Highway Administration.

Report for Task Order 4204

August 2003

ISSN 1055-1425

PROJECT TITLE:

Vehicle Lateral Control under Fault in Front and/or Rear Sensors

By

Guang Lu
Jihua Huang
Masayoshi Tomizuka

Department of Mechanical Engineering
University of California at Berkeley
Berkeley, CA 94720

Annual report for the second year of TO 4204

May 2003

Executive Summary

This report presents the research results of Task Order 4204(TO4204), *"Vehicle Lateral Control under Fault in Front and/or Rear Sensors"*, during 2000-2001. This project is a continuing effort of the Partners for Advanced Transit and Highways (PATH) on the research of passenger vehicles for Automated Highway Systems (AHS).

As all vehicles are operated automatically by computers, an AHS transforms the highway into a well-designed automatic control system with enhanced safety and capacity. An on-board computer controls each vehicle in an AHS in both longitudinal and lateral directions. Vehicle lateral control, also known as "lane-keeping" control, is to keep the vehicle in the lane laterally by controlling the steering angle at the tires. For vehicle lateral control, PATH has adopted the magnetic road reference system. Equally-spaced magnets are buried in the center of each automated lane. Magnetometers on-board a vehicle sense the magnetic field generated by each magnet. The lateral controller calculates the lateral deviation from the outputs of the magnetometers and uses this information to set the steering command.

Current PATH vehicle lateral controllers rely on the use of two sets of magnetometers on-board each vehicle, one under the front bumper, and the other under the rear bumper. Failure of magnetometers will lead to degraded mode operation and can potentially be a safety hazard. As part of an overall effort to build a reliable fault management system, TO4204 addresses the problem of developing degraded mode vehicle lateral control strategies. TO4204 is the first research project to systematically study vehicle lateral control strategies under faulty operation of the magnetometers. This project is primarily concerned with the following problems.

- lateral control of the vehicle using only one set of magnetometers
- autonomous lateral control based on a laser scanning radar sensor (LIDAR) (without the use of magnetometers)

In the previous research, controllers that use just the front magnetometers were

designed based on H_∞ optimal design techniques. In this report, since the vehicle lateral dynamics vary with the longitudinal velocity, feedback linearization has been employed to eliminate the time varying terms approximately. A mismatched observer has been designed to stabilize and tune the internal dynamics as well as to provide accurate state estimates for feedback linearization. The control system has been proved to be quadratically stable. Experimental results are presented in this report to demonstrate the effectiveness of the controller design.

Current PATH vehicle lateral controllers can no longer work if all the magnetometers on-board a vehicle stop functioning. To solve this problem, an autonomous vehicle following control scheme is developed as a back-up system to replace the current lateral controller when such a situation occurs. The new control scheme uses a laser scanning radar sensor, which measures the relative position of the controlled vehicle with respect to its preceding vehicle. With this configuration, a vehicle with on-board LIDAR can be controlled to follow the preceding vehicle without the use of any magnetometers. This controller has been successfully tested, and experimental results are presented in this report.

Previous research indicates that front magnetometers are critical for vehicle lateral control. When the front magnetometers fail, the lane-keeping performance deteriorates substantially. However, the desired vehicle performance may be achieved by combined use of the rear magnetometers with the LIDAR sensor. Although a controller design method was proposed for the combined use of the two types of sensors in the previous year, the optimal design has not been studied. In this report, a new control algorithm is proposed to achieve the optimal combined use of LIDAR and rear magnetometers. Simulation results for this algorithm are presented in this report.

Abstract

This report documents the findings of research performed under TO4204, *"Vehicle Lateral Control under Fault in Front and/or Rear Sensors"* during the year 2000-2001. The research goal of TO4204 is to develop vehicle lateral control strategies under faulty operation of the magnetometers. The main objectives of the project are: (1) to design controllers that use the output from only one set of magnetometers, and (2) to develop an autonomous lateral control scheme that uses no magnetometers.

New controllers that use just the front magnetometers have been designed based on H_∞ optimal design techniques in the previous research. In this year, the controller design has been continued by applying feedback linearization to eliminate the time varying terms caused by the variation of longitudinal velocity in the vehicle lateral dynamics. A mismatched observer has been designed to stabilize and tune the internal dynamics, and also to provide accurate state estimates for feedback linearization. Stability of the control system has been proved. Experimental results are presented to validate the controller design.

An autonomous vehicle following control scheme is developed as a back-up system to replace the current lateral controller when all magnetometers fail. The new control scheme uses a laser scanning radar sensor, which measures the relative position of the controlled vehicle with respect to its preceding vehicle, to control the vehicle to follow its preceding vehicle. Experimental results of the autonomous vehicle following control are presented in this report.

As shown in previous research, when the front magnetometers fail, the lane-keeping performance deteriorates substantially. A new back-up control system has been developed by combining the use of rear magnetometers with LIDAR. The design procedure guarantees to achieve the optimal combined use of the two sensors. Simulation results for this controller are presented in this report.

Keywords: vehicle lateral control, bicycle model, H_∞ optimal control, autonomous lateral control, vehicle following.

1 Introduction

This project focuses on vehicle lateral control subject to magnetometer failures. The current PATH lateral control algorithms rely on the outputs of two sets of magnetometers, one installed under the front bumper of the vehicle and the other under the rear bumper of the vehicle. Failures in these magnetometers lead to degraded mode operation, and can potentially be a safety hazard. TO4204 is the first research project to systematically study vehicle lateral control strategies under faulty operation of magnetometers. This project is a part of the fault management of vehicle lateral control in Automated Highway Systems. The main research topics concerned in this project are as follows.

- Developing lateral controllers that use only one set of magnetometers (when the other set of magnetometers fails).
- Developing autonomous vehicle following control schemes based on laser scanning radar sensor(LIDAR) that uses no magnetometers (when both sets of magnetometers fail).

In the previous research[5], new lateral controllers that use only the front magnetometers have been designed by applying H_∞ optimal design techniques. The controller design was based on a vehicle model with fixed dynamics. Vehicle dynamics, however, varies with the variation of vehicle's longitudinal velocity. One way of solving this problem is to introduce gain scheduling, but this will make the design complicated and it is also difficult to verify the stability of the overall control system. The controller design described in this report provides a simple yet effective controller structure. Instead of an explicit gain scheduling, feedback linearization has been employed to approximately eliminate the time varying terms in the system models. In other words, the feedback gain of feedback linearization is a function of the longitudinal velocity, and hence the controller achieves gain scheduling implicitly. Since the vehicle lateral dynamics, with the steering angle at the front tires as the control input,

and the front magnetometer output as the system output, has weakly damped zeros, matched observers such as Luenberger observer and Kalman Filter result in weakly damped internal dynamics. For the vehicle lateral dynamics, with the steering angle as the control input, and the rear magnetometer output as the system output, such matched observers result in unstable internal dynamics, due to the right-half-plane zero in the system dynamics. In this report, a mismatched observer has been designed to stabilize and tune the internal dynamics. The mismatched observer also provides accurate state estimates for feedback linearization. The resulting control system has been proved to be Quadratically Stable. Experimental results are included in this report to demonstrate the effectiveness of the controller design.

Current PATH vehicle lateral controllers can no longer work if all the magnetometers on-board a vehicle fail. An autonomous vehicle following control scheme is proposed in this report as a back-up system to replace the current lateral controller when such a situation occurs. The new control scheme uses a laser scanning radar sensor (LIDAR), which measures the relative position of the controlled vehicle with respect to its preceding vehicle. With this configuration, a vehicle with on-board LIDAR can be controlled to follow the preceding vehicle without the use of any magnetometers. However, the validity of this control scheme inevitably depends on the performance of the preceding vehicle, i.e., lateral deviation of the lead vehicle results in accumulated errors of the following vehicles, which may cause the string stability problem.

Previous research[5] indicates that front magnetometers are critical for vehicle lateral control. More precisely, if the front magnetometers fail, a right-half-plane zero appears on the pole-zero map of the dynamic system with the front wheel steering angle as input and the lateral error at the rear bumper as output. Thus, the lane-keeping performance deteriorates substantially. However, the desired vehicle performance may be achieved by combined use of the rear magnetometers with the LIDAR sensor. Under this control scheme, the controlled plant, i.e. the vehicle, becomes a

Single Input, Two Output (SITO) system: the front wheel steering angle is the input and the rear magnetometers and LIDAR define the two outputs. Interactions in such a system under closed loop control are a significant concern, in the sense that disturbances in one output may have strong effects on the other output. Freudenberg and Middleton[2] have proposed the concepts of "direction" and "alignment" in analyzing general SITO systems. This report will analyze the interactions of the SITO systems, and propose a controller design procedure to achieve minimum interactions as well as stability and optimal performance under failure of front magnetometers. This control scheme has guaranteed string stability.

This report is organized as follows. In Section 2, the vehicle lateral dynamics with and without magnetometer faults are introduced. Section 3 describes the feedback linerization and mismatched observer designed for the vehicle lateral control system that uses just one set of magnetometers. In Section 4, an autonomous vehicle following control algorithm is presented for the case where the vehicle loses information from both the front and rear sets of magnetometers. The integrated controller with combined use of LIDAR and the rear magnetometers is presented in Section 5. In Section 6, conclusions of this report are presented.

2 Vehicle Lateral Dynamics

2.1 Modeling

The simplified vehicle dynamic model (usually referred to as the bicycle model) retains the lateral and yaw motions, and neglects motion in all other directions [4]. This model can be described as a fourth order system in the standard state space form,

$$\dot{x} = Ax + B\delta + W\rho \tag{1}$$

$$x = \begin{pmatrix} y_{CG} & \dot{y_{CG}} & \epsilon_r & \dot{\epsilon_r} \end{pmatrix}^T \tag{2}$$

where x is the state variable, δ is the front wheel steering angle, and ρ is the road curvature (disturbance). y_{CG} is the lateral deviation at the vehicle CG(Center of Gravity), and ϵ_r is the relative yaw of the vehicle sprung mass relative to the road reference frame, respectively. The system matrices are

$$A = \begin{pmatrix} 0 & 1 & 0 & 0 \\ 0 & -\frac{a_{11}}{\dot{x}} & a_{11} & \frac{a_{12}}{\dot{x}} \\ 0 & 0 & 0 & 1 \\ 0 & -\frac{a_{41}}{\dot{x}} & a_{41} & \frac{a_{42}}{\dot{x}} \end{pmatrix} \tag{3}$$

$$B = \begin{pmatrix} 0 \\ b_{21} \\ 0 \\ b_{41} \end{pmatrix} \tag{4}$$

$$W = \begin{pmatrix} 0 \\ w_{21} \\ 0 \\ w_{41} \end{pmatrix} \tag{5}$$

$$a_{11} = (\phi_1 + \phi_2), a_{12} = \phi_1(d_s - l_1) + \phi_2(d_s + l_2) \tag{6}$$

$$a_{41} = \frac{l_1 C_{\alpha_f} - l_2 C_{\alpha_r}}{I_z} \tag{7}$$

$$a_{42} = \frac{l_1 C_{\alpha_f}(d_s - l_1) + l_2 C_{\alpha_r}(d_s + l_2)}{I_z} \tag{8}$$

$$b_{21} = \phi_1, b_{41} = \frac{l_1 C\alpha_f}{I_z} \tag{9}$$

$$w_{21} = -\frac{{l_1}^2 C_{\alpha_f} + {l_2}^2 C_{\alpha_r}}{I_z} \tag{10}$$

$$w_{41} = \phi_2 l_2 - \phi_1 l_1 - \dot{x}^2 \tag{11}$$

The physical meaning and values of the symbols used in the above equations are listed in Table 1.

Table 1: Vehicle Parameters

Symbols	Physical Meaning	Value
m	mass	$1485kg$
L	relative longitudinal distance between vehicles	$5m$
d	Distance of rear bumper to CG	$2.1m$
I_z	yaw moment of inertia	$2872kg/m^2$
C_f	front wheel cornering stiffness	$42000N/rad$
C_r	rear wheel cornering stiffness	$42000N/rad$
l_1	distance between front wheel and the CG	$1.1m$
l_2	distance between rear wheel and the CG	$1.58m$

2.2 Frequency domain analysis of vehicle lateral control under fault in one set of magnetometers

The current PATH lateral control algorithms employ two sets of magnetometers to implement the virtual look-ahead scheme [3][6]. According to this scheme, a lateral error (called virtual lateral error) at some distance d_s (look-ahead distance) ahead of the vehicle is constructed from the outputs of the two sets of magnetometers (front and rear magnetometers). The control objective is to minimize the virtual lateral error. In other words, the virtual look-ahead scheme is trying to minimize the lateral error at some distance ahead of the vehicle.

A frequency domain analysis shows that as the look-ahead distance d_s increases the phase lead enhances (Fig. 1). Therefore, large look-ahead distances result in increased phase lead, which significantly eases the controller design. This effect of the look-ahead distance is the main advantage of the virtual look-ahead scheme. However, if magnetometer failures occur, the look-ahead distance decreases to certain fixed values. Under fault in front magnetometers, only the lateral error at the rear magnetometers is available. Thus, the look-ahead distance d_s decreases to $-l_2$ (l_2 is the distance between the mass center and the rear bumper). Similarly, under fault in rear magnetometers, the look-ahead distance decreases to l_1 (the distance between the mass center and the front bumper). In both cases, the look-ahead distance is small and the phase lead in the system is not adequate. Figures 2 and 3 show the frequency responses from the steering input δ to the lateral error at the front bumper y_{sf} and at the rear bumper y_{sr} when the longitudinal velocity is $30m/s$. The decrease of phase lead increases the difficulty in the controller design, especially for the system with front magnetometer failure.

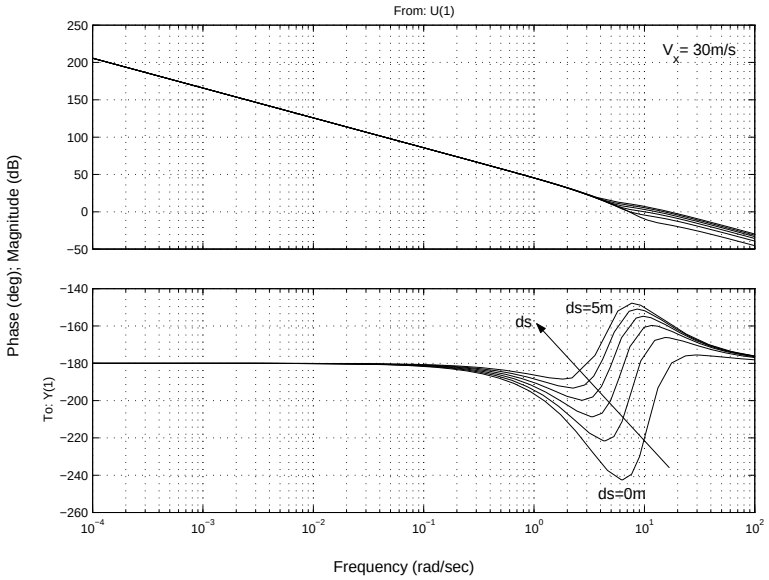

Figure 1: Bode plot of G_v (the TF from the steering input to virtual lateral error)

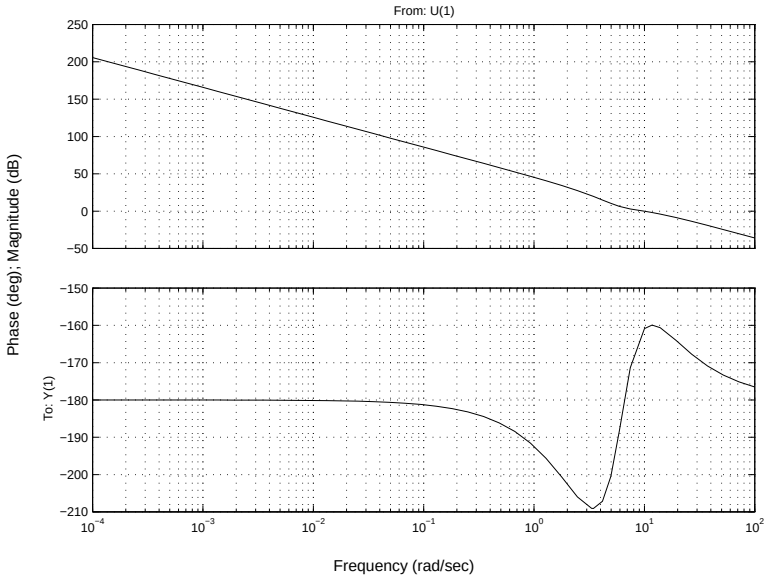

Figure 2: Bode plot of G_f (the TF from the steering input to y_{sf})

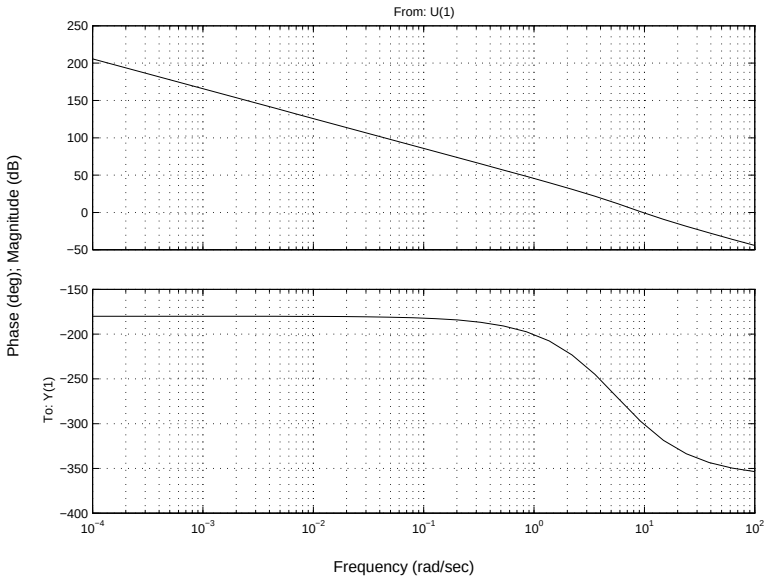

Figure 3: Bode plot of G_r (the TF from the steering input to y_{sr})

3 Vehicle Lateral Control Based on Front Magnetometers

3.1 LTV controller design based on Feedback Linearization with Mismatched Observer

3.1.1 Basic Ideas

Feedback linearization has been recognized as a powerful method for nonlinear or time varying systems. Hence, it is natural to apply feedback linearization to the vehicle lateral control system, which is an LTV (Linear Time Varying) system. It is expected that feedback linearization will cancel out the time varying terms in vehicle dynamics and work as a gain scheduling part in the controller. Since feedback linearization requires the use of all state variables and yet some vehicle state variables are not available for measurements, observers have to be designed to obtain state estimates. Generally, linear observers, such as Luenberger observer and Kalman filter, and most

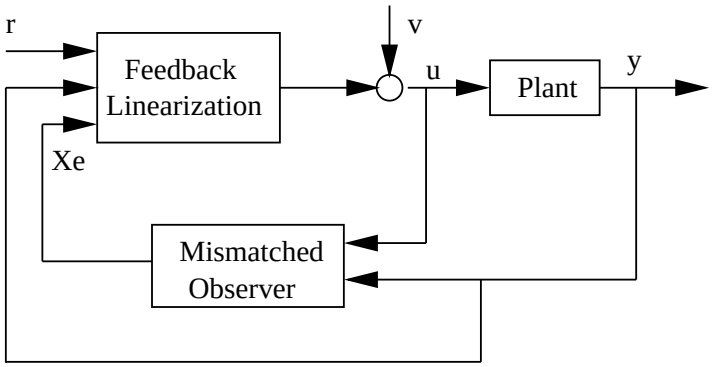

Figure 4: Closed-loop configuration with the mismatched observer

nonlinear observers are matched observer, in the sense that the observers have exactly the same structure and coefficients as the plant. It is a well-known fact that the open-loop zeros of the plant will be contained as the closed-loop poles of the internal dynamics with the use of these matched observers. As shown in the previous Section, the front magnetometer based (FMB) vehicle lateral dynamics have weakly damped zeros, therefore, by using either state feedback or matched observer feedback, the internal dynamics will also become weakly damped. There are two possible ways to solve this problem, one is to eliminate the internal dynamics, the other is to use mismatched observers for state estimation. The former way implies that we need to change the output to have relative degree 0, which is not practical in our case. The latter way is to design an observer, which can provide fairly accurate state estimates without leaving the open-loop zeros as the internal dynamics modes. That is, the observer should be able to contribute well-damped and fast closed-loop modes, as well as to estimate the states accurately. Figure 4 shows the overall closed-loop configuration of feedback linearization with a mismatched observer.

In design, the observer should not be matched, otherwise, the open-loop zeros will be trapped in the internal dynamics, i.e. the structure of the observer does not depend on the plant any more. It may be true that such a mismatched observer will not be able to provide state estimates as accurate as matched observers can, but the

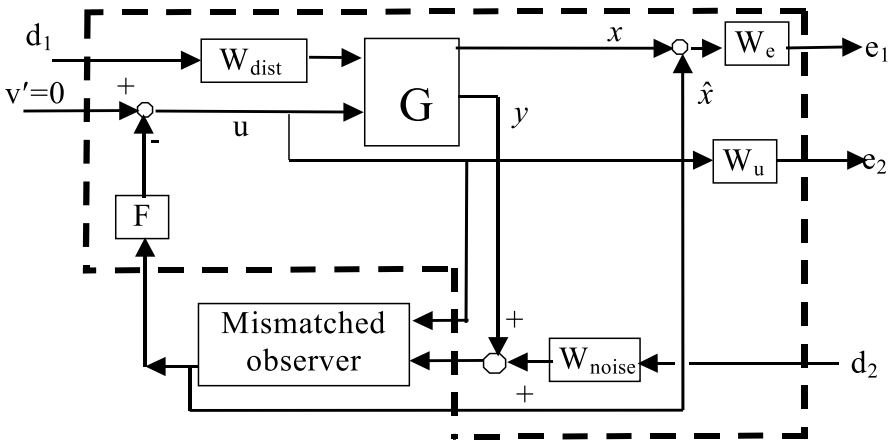

Figure 5: The H-infinity synthesis of the mismatched observer

sacrifice is made in order to bring the benefits of better closed-loop modes. Although there may be many ways to design this mismatched observer, H_∞ optimal control techniques are employed in the design. Since one main objective of the observer is to estimate the states accurately, the H_∞ synthesis is to minimize the H_∞ norm of the transfer function from the disturbances and sensor noises to the estimation errors. The overall closed-loop behavior is shaped by appropriate weighting functions. Figure 5 shows the H_∞ synthesis for the design of the mismatched observer.

For the regulation problem, the desired trajectory is always 0, therefore, $v'(t) = 0$.

3.1.2 The Controller Design based on Feedback Linearization with Mismatched Observer

Feedback Linearization

The relative degree of the vehicle lateral dynamics is 2; therefore, the desired closed-loop system is of 2nd order, which can be written as:

$$\ddot{y}_f + k_1\dot{y}_f + k_2 y_f = v'(t) = 0$$

Since it is a regulation problem, $v'(t) = 0$. Based on the desired closed-loop dynamics, the control input can be easily derived:

$$\delta = \frac{-k_1\dot{y}_f - k_2 y_f - (A_2 + d_f A_4)\hat{X} + v'(t)}{b_{21} + d_f b_{41}} \tag{12}$$

where A_2 and A_4 are the second and fourth row of the A matrix in the state equations (Eq. 1), and $\hat{X}$ is the state estimates given by the mismatched observer. Notice that the feedback gains are functions of A matrix, which varies with the longitudinal velocity; therefore, the feedback gains also vary with the longitudinal velocity.

Design of the Mismatched Observer

The H-infinity synthesis is shown in Figure 5. Both the road curvature and the sensor noise are regarded as disturbances. In order to provide accurate estimates for feedback linearization, the difference between the states and their estimates is treated as an error to be minimized. The control force δ is also treated as an error to avoid actuator saturation and excitation of high frequency modes.

H-infinity controller design significantly relies on the choice of proper weighting functions. The weighting functions in the mismatched observer design have been chosen as follows:

- Modeling of the lateral disturbance $\dot{\epsilon}_d$

  The lateral disturbance $\dot{\epsilon}_d$ in Eqs. (2) and (3) can be modeled from the road curvature ρ by:

  $$\dot{\epsilon}_d = \rho v_x \tag{13}$$

  where v_x is the longitudinal velocity. The maximum magnitude of the road curvature is set to be $1/(800m)$ in H_∞ synthesis, which is steeper than the general curvature disturbances on highways (less than $1/(1000m)$). (The larger the curvature ρ is, the sharper the curve is). Since the road curvature does not change frequently on highways, the disturbance can be modeled as a band-limited signal. Here, in order to keep the order of the controller small, the order

of the disturbance model is zero:

$$W_{dist} = \frac{v_x}{800} \tag{14}$$

- Modeling of magnetometer noise

  Since the measurement noise generally has high frequency components, the weighting function on noise should be a high pass filter. But in consideration of the order of the resulting controller, the noise weighting function is chosen to be a constant.

$$N_{y_s} = \frac{1}{200}$$

- Penalty on the estimation error

  There are four states, hence there are four weighting functions, each on one state estimation error. Let's first consider the weighting function on estimation error of lateral deviation at vehicle CG, i.e. x_1. The weighting function will have similar requirement as that for lateral error y_f. The high frequency component of the lateral error measurement is considered as noise. This is because the road curvature is piecewise continuous and the vehicle dynamics contains mainly low frequency dynamics. Thus the penalty is set high on the low frequency component of the lateral error measurement.

$$W_y = 50\frac{s+0.2}{s+0.1} \tag{15}$$

  We are more concerned with the accuracy of the lateral deviation and yaw angle, therefore, the weightings on lateral deviation derivative and yaw rate are simply set to 1. Considering $y_f = x_1 + d_f x_3$, the weighting on yaw angle x_3 is d_f times of the weighting on x_1, the lateral deviation at vehicle CG. Hence the weighting function on estimation error is:

$$W_e = \begin{bmatrix} W_y & 0 & 0 & 0 \\ 0 & 1 & 0 & 0 \\ 0 & 0 & d_f W_y & 0 \\ 0 & 0 & 0 & 1 \end{bmatrix} \tag{16}$$

- Penalty on the control input δ

  The high frequency component of the control force must be restricted because it may saturate the actuator and excite the unmodeled high frequency dynamics. Therefore, the penalty is set high at high frequencies, and the bandwidth of the controller is restricted to be lower than that of the actuator (which is around 5Hz). To avoid excitation of suspension mode, a high penalty is added at $5Hz$, which is realized by an inverse of a notch at $5Hz$.

$$\begin{aligned} W_\delta &= W_{actuator} \times W_{suspension} \\ &= 1500\frac{s+10}{s+100} \times \frac{s^2+10\pi s+(10\pi)^2}{s^2+1.6\pi s+(10\pi)^2} \end{aligned} \tag{17}$$

Synthesis Result

The designed mismatched observer is fifth order, and the resulting controller is the combination of the feedback linearization and the mismatched observer. Notice that the feedback gain changes as the longitudinal velocity changes, while the mismatched observer is fixed. Hence the implementation of the controller is much simpler than the general gain scheduled controllers. Figure 6 shows the resulting controller. The controller provides more phase to compensate the increasing phase lag of the vehicle lateral dynamics as the longitudinal velocity increases.

3.2 Discussion on Stability

At first glance, it may easily be assumed that the closed-loop system will definitely be stable since H_∞ optimal control technique is applied. However, even with exact state feedback, feedback linearization only results in a LTI input-output relationship, leaving the internal dynamics still time varying. Therefore, to design the mismatched observer based on H_∞ techniques, the internal dynamics should still be fixed (in the present case, the velocity is fixed to be $20m/s$ for the observer design). Consequently, the H_∞ technique will only guarantee closed-loop stability at this fixed velocity (i.e.

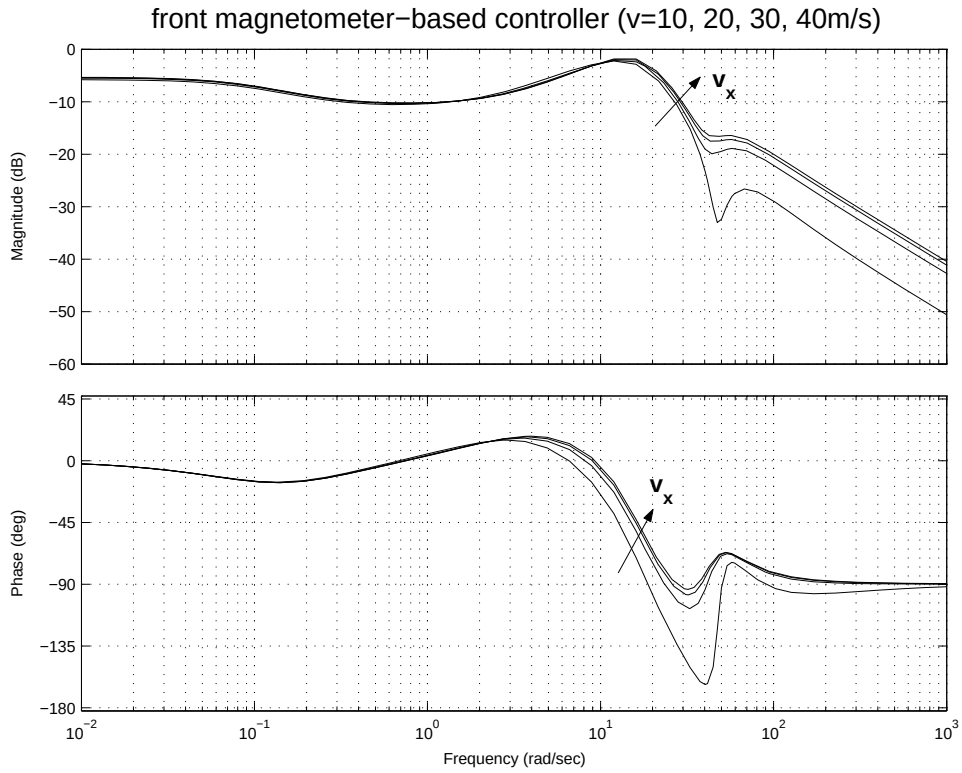

Figure 6: The resulting controllers

$v_x = 20m/s$); there is no guarantee for stability in the whole operating range ($0 < v_x < 40m/s$).

To analyze the stability in the whole operating range, the concept of Quadratic Stability (QS) is utilized. According to [7], we define the Linear Parameter Varying (LPV) systems and the Quadratic Stability of LPV systems as follows:

Definition: Linear Parameter Varying (LPV) System

Assume that the following are given:

- *a compact set* $P \subset R^s$,
- *a function* $A \in C^0(R^s, R^{n\times n})$,
- *a function* $B \in C^0(R^s, R^{n\times n_d})$,
- *a function* $C \in C^0(R^s, R^{n_e\times n})$, *and*
- *a function* $D \in C^0(R^s, R^{n_e\times n_d})$.

where $C^0(U, V)$ *is a set of continuous functions from* U *to* V, R^s *is s-dimension real vector space, and* $R^{n\times n}$ *denotes n-by-n real matrix. An n-th order linear parameter varying (LPV) system is the one whose dynamics evolves as:*

$$\begin{bmatrix} \dot{x}(t) \\ e(t) \end{bmatrix} = \begin{bmatrix} A(\rho(t)) & B(\rho(t)) \\ C(\rho(t)) & D(\rho(t)) \end{bmatrix} \begin{bmatrix} x(t) \\ d(t) \end{bmatrix} \tag{18}$$

where $\rho \in F_P$, $x(t)$, $\dot{x}(t) \in R^n$, $d(t) \in R^{n_d}$ *and* $e(t) \in R^{n_e}$ Note: As the matrix functions A, B, C and D are continuous functions of parameter ρ, they are, in fact, norm-bounded on the compact set P.

Definition: Quadratic Stability

Given a compact set $P \subset R^s$, *and a function* $A \in C^0(R^s, R^{n\times n})$, *the function* A *is quadratically stable over* P *if there exists a matrix* $P \in S_+^{n\times n}$ *(Positive Definite n-by-n matrix), such that for all* $\rho \in P$

$$A^T(\rho)P + PA(\rho) < 0 \tag{19}$$

Definition: Quadratic Stability of LPV systems

For LPV systems defined in the above definition, if A is quadratically stable (QS) over P, then the system is a quadratically stable LPV system.

In other words, a LPV system is quadratically stable if its system matrix $A(\rho(t))$ is Hurwitz for all $\rho \in P$. For vehicle lateral control, the corresponding varying parameter is the longitudinal velocity v_x, and the set $P = v_x : 0 < v_x < 40$. To verify that the closed-loop system is indeed QS, we will first show that the closed-loop system is a LPV system, and then we will prove that its system matrix $A_clp(v_x(t))$ is Quadratically stable. After we derive the closed-loop system matrix, it is then easy to verify that the closed-loop system matrix A_{clp} is indeed Hurwitz, hence, the closed-loop system is Quadratically Stable.

3.3 Experimental Result

Experiments have been conducted at Richmond Field Station at the University of California, Berkeley. The test vehicle was a Buick LeSabre. The controller after fine tuning is shown in Fig.7. Compared with Fig.6, the main difference is the low frequency gain which is changed by modifying the feedback gain. After fine tuning (mainly the changes on low frequency gain), the controller achieved the performance shown in Fig.8. ρ is the road curvature at Richmond Field Station. Here the largest and smallest radius of the curve are about $480m$ and $220m$ respectively, which is really small compared with the radius of general highway which is larger than $1000m$. y_f and y_r are the measurement of front magnetometers and rear magnetometers. For longitudinal velocity up to $16m/s$, the maximum lateral error is around $0.1m$ (the largest one at the beginning is the initial lateral error depending on the initial position of the vehicle relative to the road centerline, hence can not be counted as the controlled lateral error). The steady state lateral error on a straight lane is smaller than $0.02m$. From the steering input δ, we can also observe that the steering is rather smooth, with the high frequency component around $1Hz$.

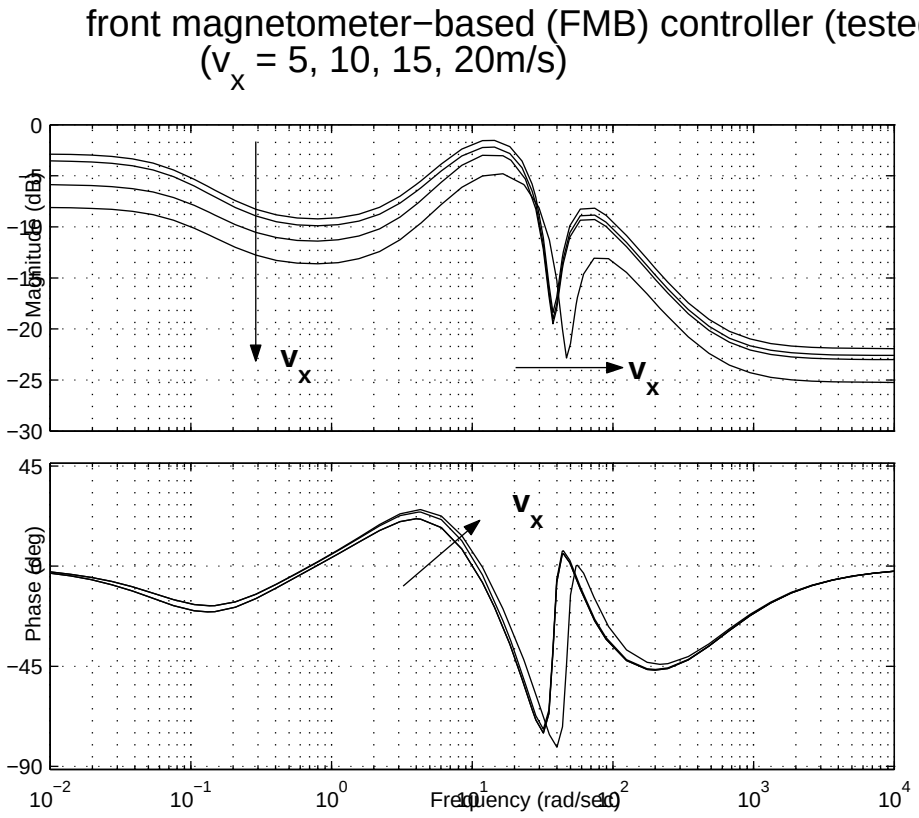

Figure 7: The controllers tested in the experiments

The vehicle is tested up to $20m/s$ at Richmond Field Station, and the performance is quite satisfactory. Since the route at Richmond Field Station only allows low speed testing, high speed testing at Crows Landing is current being scheduled.

4 Autonomous Vehicle Following Using LIDAR

4.1 Laser Scanning Radar Sensor (LIDAR)

4.1.1 LIDAR Working Scheme

The LIDAR sensor has been installed on the top of the controlled vehicle as shown in Figs.9 and 10. As shown in Fig.11, a laser scanning radar sensor consists of a laser diode, a laser receiver, and a scanning mechanism. The laser diode emits laser beams,

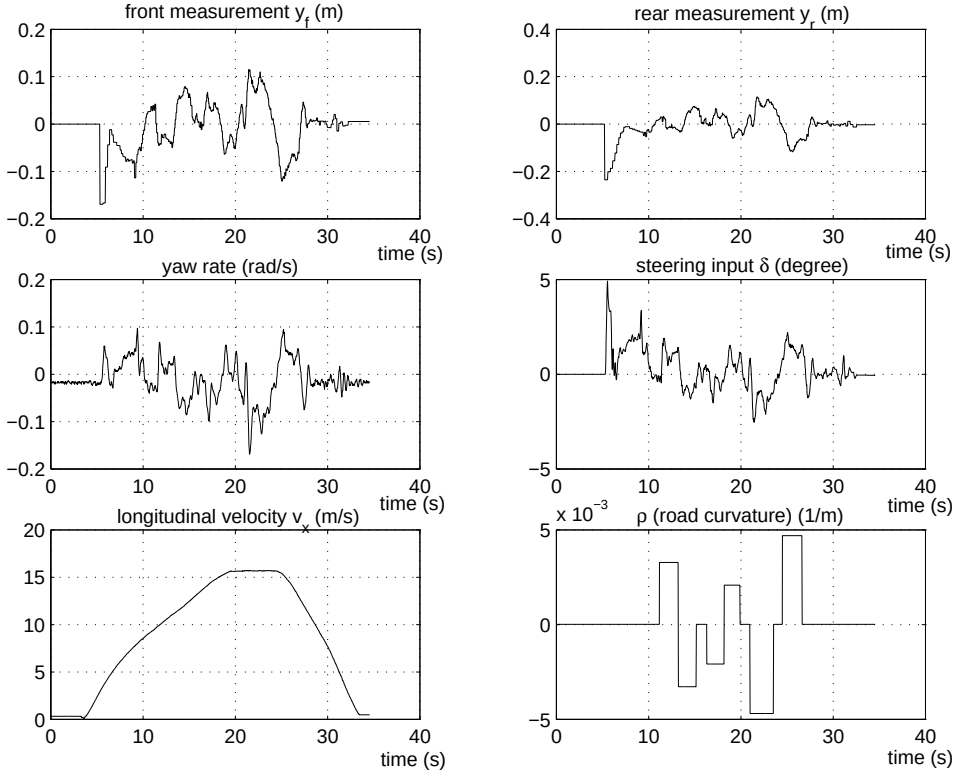

Figure 8: The experimental result (testing vehicle: Buick Lesabre)

Figure 9: LIDAR mounted on the top of the vehicle

which are bounced back if they hit any reflective surfaces of the surrounding objects. The reflected laser beams are detected by the laser receiver. The scanning mechanism is usually a rotating prism, and it allows the laser beams to scan a certain range of angle. Only reflective objects within this range are detectable by the LIDAR sensor. The distance to an object is measured based on the Time-Of-Flight (TOF) principle, which says:

$$distance = flight\ time \times speed\ of\ the\ light \tag{20}$$

where speed of the light is 2.976×10^8 m/s. The lateral position of the object is determined from the distance and the angle of scanning.

4.1.2 Data Processing

The laser beam emitted by the LIDAR sensor used here scans horizontally 12^o in 80 steps. At each step, the LIDAR sensor measures the distance and angular position of the object that reflects the laser beams along with the intensity of the reflection. Therefore at each sampling point, the returned sensor measurements are 80 sets of

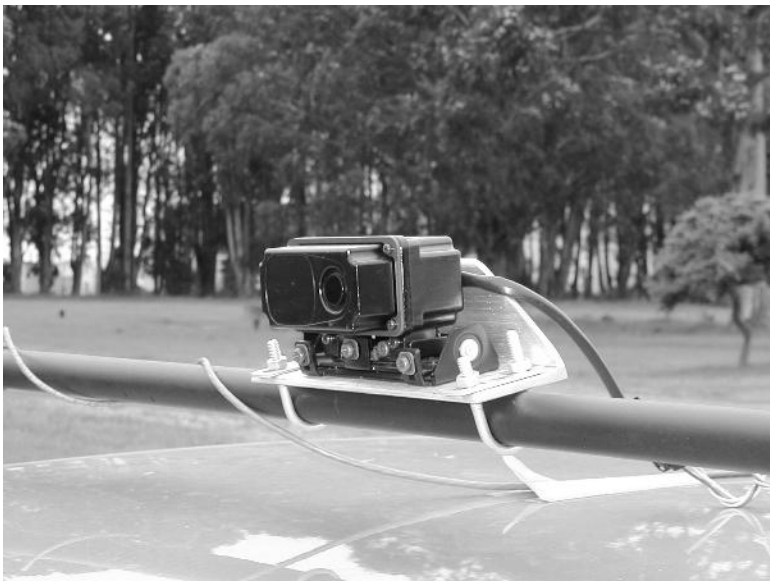

Figure 10: LIDAR: a closer look

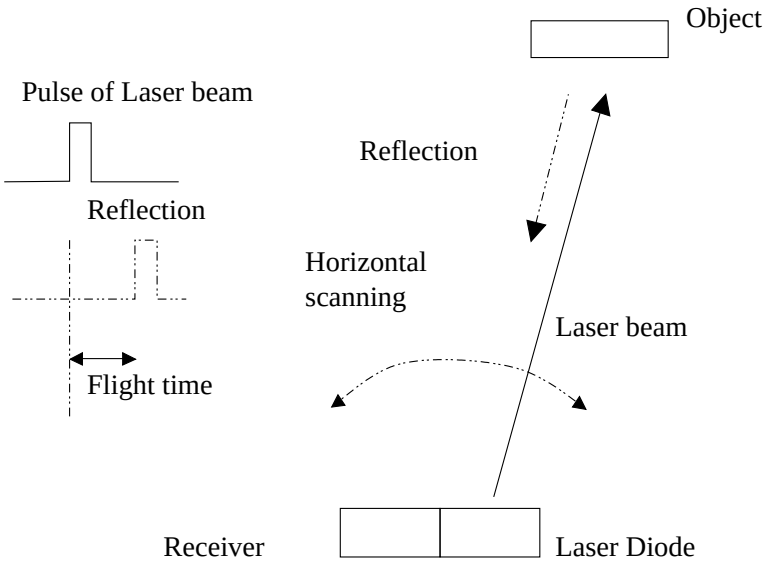

Figure 11: LIDAR working scheme

distance, angular position, and intensity. To determine the actual position of the target of interest, a probability data association method proposed by Bar-Shalom[1] has been applied to process the LIDAR measurements. The target motion is described as

$$x[k+1] = A_s x[k] + B_{ws} w[k] \tag{21}$$

where $w[k]$ is the normally distributed, zero mean, white process noise, and

$$x[k] = [x_{target}, \dot{x}_{target}, y_{target}, \dot{y}_{target}]^T \tag{22}$$

$$w[k] = \begin{pmatrix} w_x[k] \\ w_y[k] \end{pmatrix} \tag{23}$$

$$A_s = \begin{pmatrix} 1 & T_s & 0 & 0 \\ 0 & 1 & 0 & 0 \\ 0 & 0 & 0 & T_s \\ 0 & 0 & 0 & 1 \end{pmatrix} \tag{24}$$

$$B_{ws} = \begin{pmatrix} \frac{T_s^2}{2} & 0 \\ T_s & 0 \\ 0 & \frac{T_s^2}{2} \\ 0 & T_s \end{pmatrix} \tag{25}$$

The LIDAR measurements arrive in polar coordinates and are converted to Cartesian. Accordingly, the measurement model is given by

$$z[k] = H_s x[k] + v[k] \tag{26}$$

where $v[k]$ is the zero mean, white, Gaussian measurement noise which is independent of $w[k]$ and $x[0]$.

$$H_s = \begin{pmatrix} 1 & 0 & 0 & 0 \\ 0 & 0 & 1 & 0 \end{pmatrix} \tag{27}$$

$$v[k] = \begin{pmatrix} v_x[k] \\ v_y[k] \end{pmatrix} \tag{28}$$

At time index k, LIDAR returns 80 measurements, denoted as $\{z_i[k]\}_{i=1}^{80}$. The best estimate of the target's state is the conditional mean based upon all the observations that with some nonzero probability originated from the target. For simplicity, the probability density of the state conditioned upon past observations is assumed normal with mean $\hat{x}_{k|k-1}$ and covariance $P_{k|k-1}$. Denote the probability of the $z_i[k]$ being the correct measurement at time index k as $\beta_i[k]$. The prediction equations are

$$\hat{x}[k|k-1] = A_s\hat{x}[k-1|k-1] \tag{29}$$

$$\hat{z}[k|k-1] = H_s\hat{x}[k|k-1]. \tag{30}$$

For m_k validated measurements, the state estimation equation is

$$\hat{x}[k|k] = \hat{x}[k|k-1] + F[k]v[k] \tag{31}$$

where

$$v[k] = \sum_{i=1}^{m_k} v_i[k]\beta_i[k] \tag{32}$$

$$v_i[k] = z_i[k] - \hat{z}[k|k-1] \tag{33}$$

$$F[k] = P[k|k-1]H_s^T S^{-1}[k] \tag{34}$$

$$S[k] = H_s P[k|k-1]H_s^T + V[k] \tag{35}$$

The estimation error covariance is

$$\begin{aligned} P[k|k] = \beta_0[k]P[k|k-1] + (1-\beta_0[k](I - F[k]H_s) \\ P[k|k-1]F[k][(\textstyle\sum_{i=1}^{m_k} v_i[k]v_i^T[k]\beta_i[k]) - v[k]v^T[k]]F^T[k] \end{aligned} \tag{36}$$

The probability weightings $\beta_i[k]$ are computed by using Bayes' Rule and considering intensity data of each measurement.

4.2 Design Issues

The main difference between vehicle following and road following is due to the coordinate frames where the sensor measurements are obtained from. In road-following

control, on-board sensors, either magnetometers or vision sensors, measure the position of the vehicle with respect to an absolute coordinate frame (e.g. road reference frame), while in vehicle-following control, the sensors such as LIDAR can only measure the ego-vehicle's position relative to another moving vehicle. Thus the fundamental issue in designing a vehicle-following control system is to decide the desired trajectory of the ego-vehicle. Once the desired trajectory of the ego-vehicle is determined, there is not much difference between the designs for vehicle-following and road-following controllers because the vehicle dynamics are the same, despite the data manipulation of different types of sensors.

In terms of how to generate the desired trajectory, several schemes have been proposed by previous researchers. The ego-vehicle may go through a straight line towards the lead vehicle, or negotiate a curve which is predefined by the computer to reach the lead vehicle, or follow the trajectory of the lead vehicle point by point by storing the relative position data from the on-board sensors. In this report, the ego-vehicle is controlled to follow directly the lead vehicle according to the information from LIDAR. The input signal into the controller is the relative lateral distance of these two vehicles, and the LIDAR is considered as simply a sensor which provides larger look-ahead distance. The controller used here is:

$$\frac{(2s+1)(18s+1)}{(0.2s+1)(56.98s+1)} \tag{37}$$

The Bode plot of this controller is shown in Fig.12.

A reasonable question concerning this type of controller design is how L, the look-ahead distance, affects the system performance. As shown in Fig.13, while the controller uses the deviation error of the following vehicle at L distance ahead as the feedback, the ego-vehicle tends to cut the curve, and the system error of using this method can be calculated quantitatively. In this figure, L is the distance between the two vehicles, R is the road radius, and α is the angle as shown. It is known that the road curvature of highways cannot be larger than 0.00125 $[1/m]$; then the worst-case

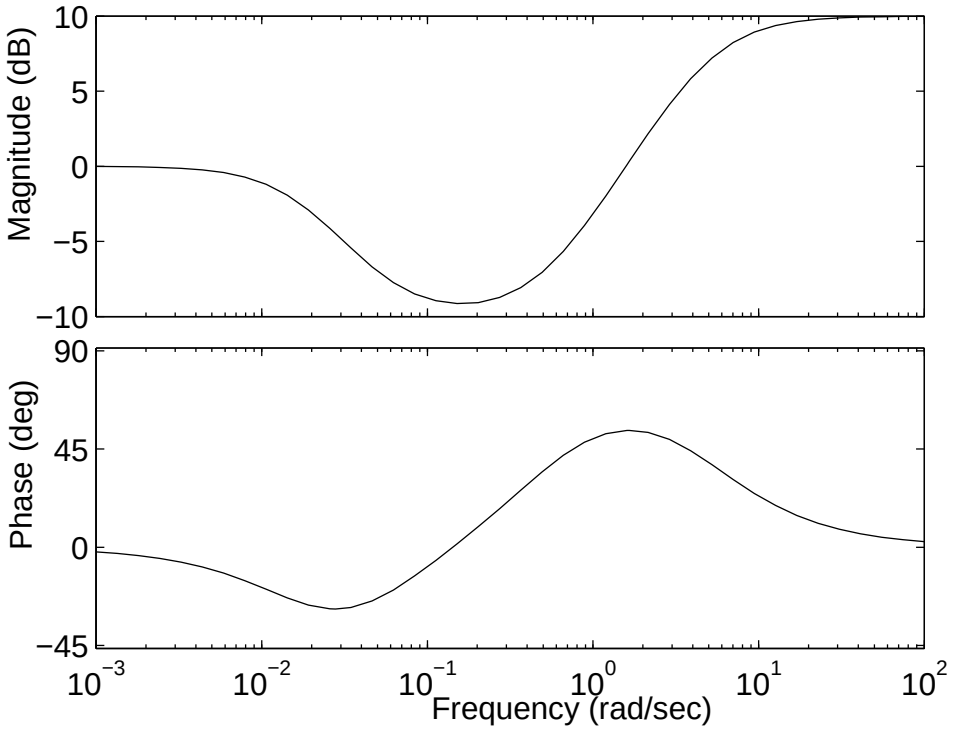

Figure 12: Bode plot of the autonomous vehicle following controller

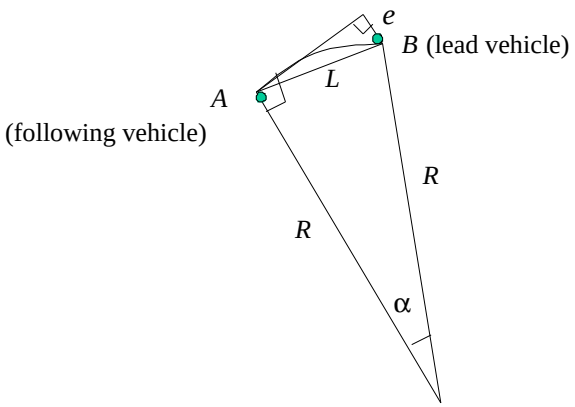

Figure 13: System error of the control scheme

system error is:

$$e = \frac{L^2}{2R} \tag{38}$$

Since most current PATH lateral controllers use a look-ahead scheme, i.e. the controllers compute lateral deviation at a distance ahead of vehicle CG, the worst-case system error for the vehicle following scheme compared to the look-ahead scheme is only

$$e_r = \frac{L^2 - d^2}{2R} \tag{39}$$

where d is the look-ahead distance used by PATH lateral controllers.

Assuming d as 4 m, which is a reasonable look-ahead distance in controller design, the worst-case system error (when R is 800 m) is 5 cm for $L = 10$ m. Thus for small following distance, this control scheme is acceptable. The Bode plots of the open loop transfer function from the steering input to the lateral displacement of the vehicle are shown in Fig.14.

4.3 Experimental Results

Experiments have been conducted on a platoon of two Buick vehicles on a test track at the Richmond Field Station in California. The lead vehicle was under PATH magnetometer-based control in lateral direction, and the following vehicle used the

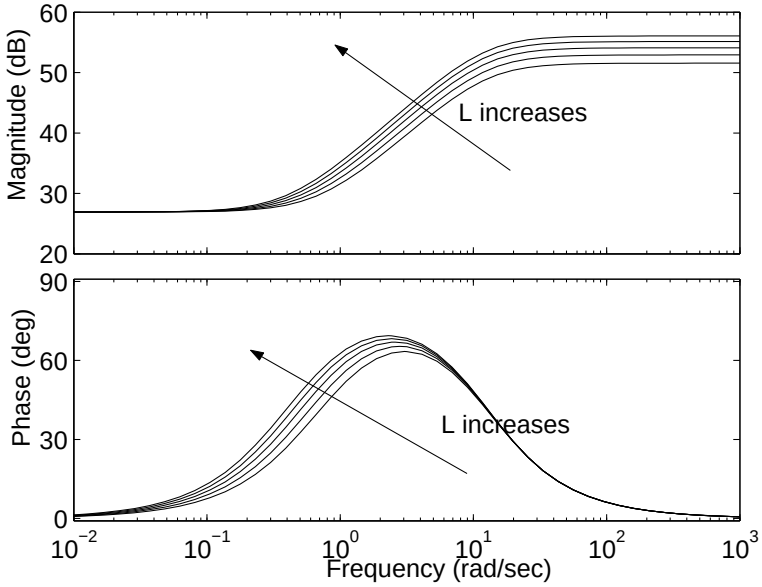

Figure 14: Effects of look-ahead distance on the open loop system dynamics (for vehicle velocity $= 8m/s$, and $L = 8, 10, 12, 14, 16m$)

Figure 15: Autonomous vehicle following experiment (the vehicle in the center of the picture is the lead vehicle; the vehicle at the bottom of the picture, which is not shown completely, is the following vehicle)

control algorithm described in this section. Both vehicles were under manual control by drivers in the longitudinal direction. The space between these two vehicles was controlled manually by the driver who operated the following vehicle. The vehicle speed was maintained at about 20 MPH and the space between these two vehicles was expected to be kept at about 10 m. The test track was a curved lane with magnetic markers buried in the center. The road curvature of the test track was 3 to 4 times larger than that of highways. Magnetometer readings were collected in order to evaluate the performance of the autonomous vehicle following control scheme, but they were not used for control. The vehicle lateral controller just used the measurements from LIDAR and set the steering command according to the control algorithm. Note that there were two sets of magnetometers on-board each vehicle, one under the front bumper, and the other under the rear bumper. Figures 16 and 17 show the experimental results of the controlled vehicle. The vehicle following performance is evaluated by the measurements from both the LIDAR and the magnetometer sensors. It can be seen from the results that the controlled vehicle is still kept in the lane by following a lead vehicle. The experimental results of the lead vehicle are shown in Fig.18. It can be concluded from the results that the tracking error of the front vehicle has been magnified on the following vehicle. This may cause the string stability problem if the vehicle following algorithm is applied to many vehicles in a platoon. This problem is solved in the next section by combining the use of LIDAR and rear magnetometers.

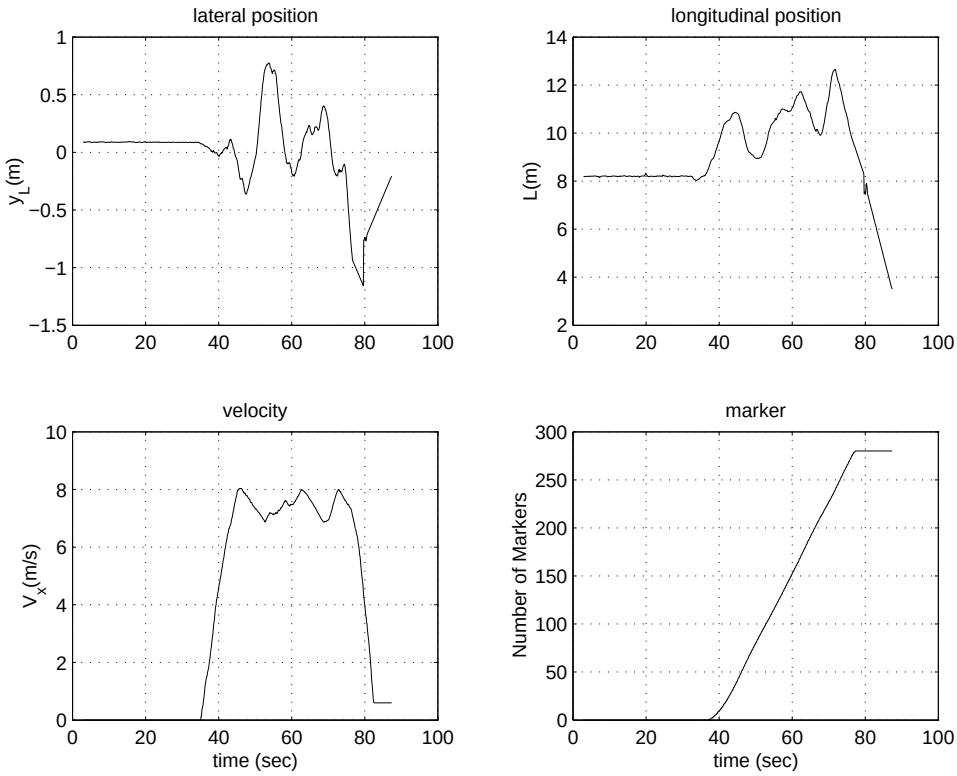

Figure 16: Experimental results of following vehicle: lateral and longitudinal distance measured by LIDAR sensor, vehicle velocity, and recording of magnetic markers

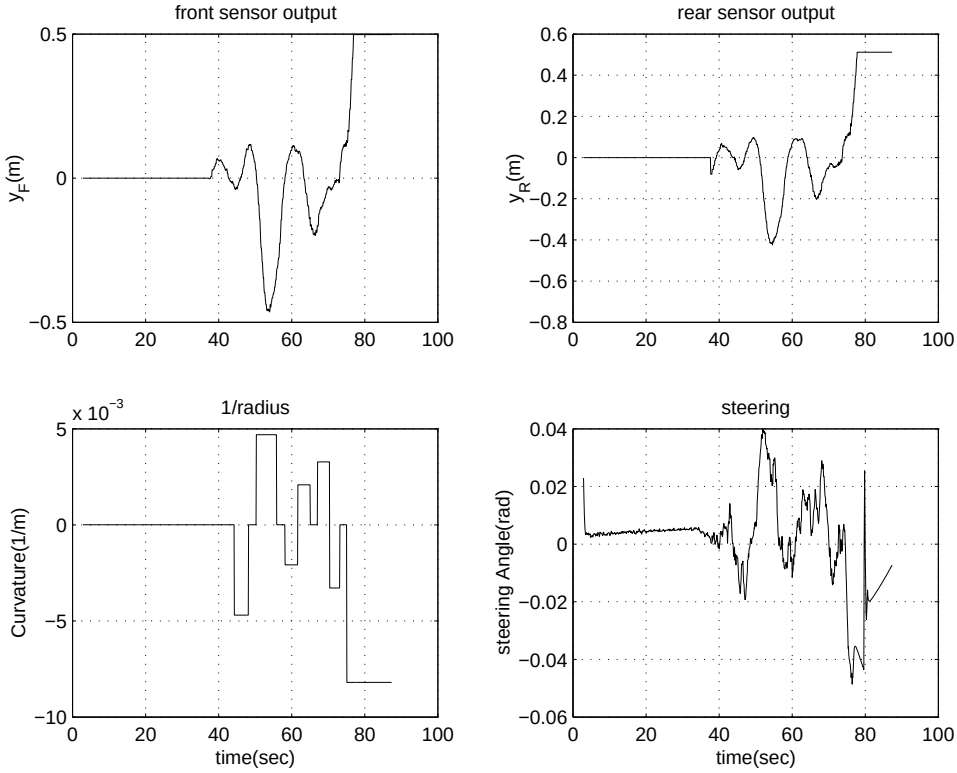

Figure 17: Experimental results of following vehicle: measurements from front and rear magnetometers, road curvature, and steering angle

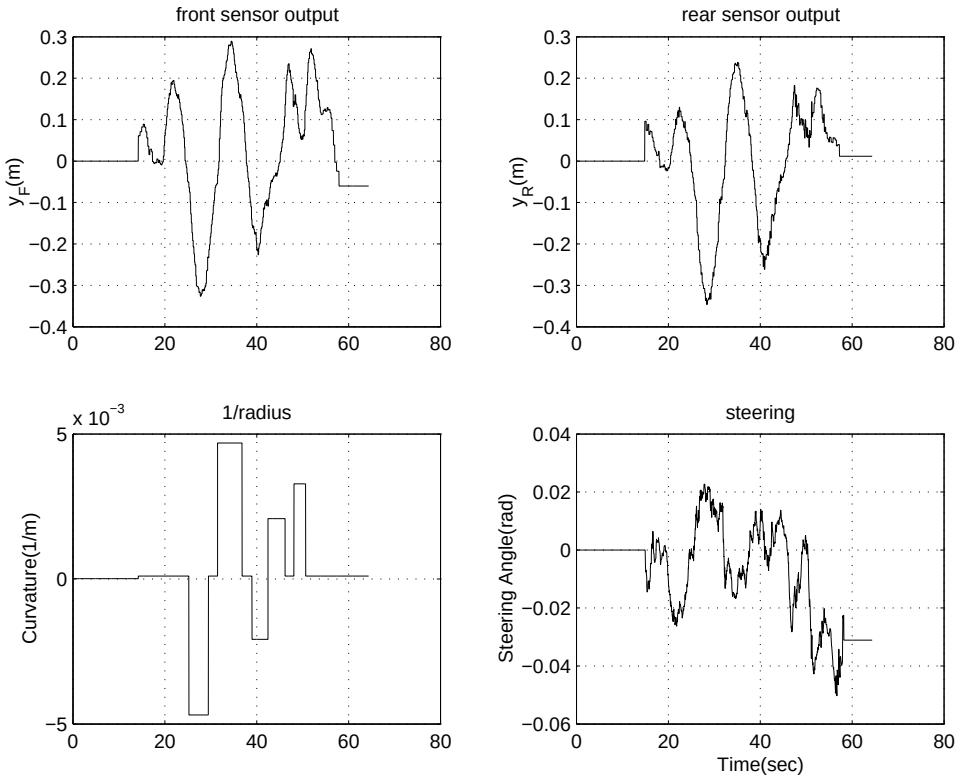

Figure 18: Experimental results of lead vehicle: measurements from front and rear magnetometers, road curvature, and steering angle

5 Autonomous Vehicle Following with Combined Use of LIDAR and Rear Magnetometers

5.1 Problem Formulation and Control Objectives

When the front magnetometers fail, the back-up system may utilize the rear magnetomters and the LIDAR sensor. It should be noted that the measurements of the LIDAR sensor are relative to the coordinate system fixed to the lead vehicle, while those of the rear magnetometers are relative to the road reference coordinate system. In road reference system, LIDAR measurements can be considered as the composition of two parts, i.e. the position of following vehicle at the LIDAR location and the position of the rear of the preceding vehicle. The latter part depends on the dynamics of the preceding vehicle. It is assumed in this report that there is no communication between the vehicles, and the dynamics of the preceding vehicle are considered as unknown disturbances. Hence, the system outputs can be written as $y = Hx$, where

$$H = \begin{bmatrix} 1 & 0 & L & 0 \\ 1 & 0 & -d & 0 \end{bmatrix}, \tag{40}$$

and y is the measured system output. The physical meanings of L and d can be found in Table 1. The first system output in the above equations is the measurement from the LIDAR sensor and the second one is from the rear magnetometers. Figure 19 shows the geometry of the sensor locations and measurements. Note that the output equation assumes that the LIDAR output of the following vehicle is equivalent to the lateral error measured by a (virtual) sensor located at L $[m]$ ahead of the following vehicle's CG. Disturbance d_1 is introduced to absorb the discrepancy between this assumption and the actual situation. The dynamics of the preceding vehicle may affect d_1. The control system is shown in Fig.20, where P is the Single Input, Two Output (SITO) plant, y_L is the output of the LIDAR sensor, d_1 is the disturbance due to the unknown actual position and dynamics of the preceding vehicle, and d_2 is the

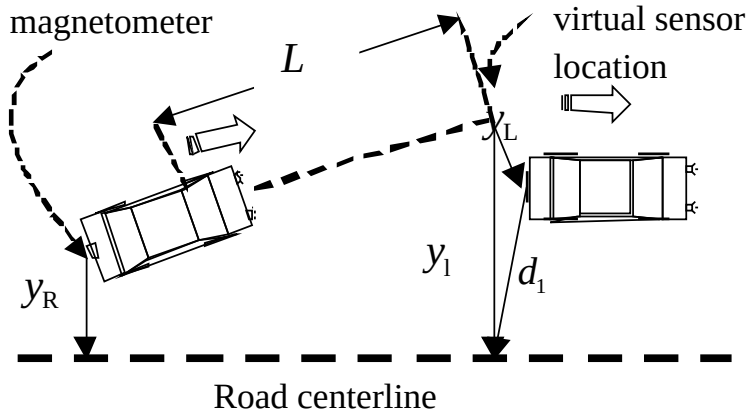

Figure 19: Geometry of sensor locations

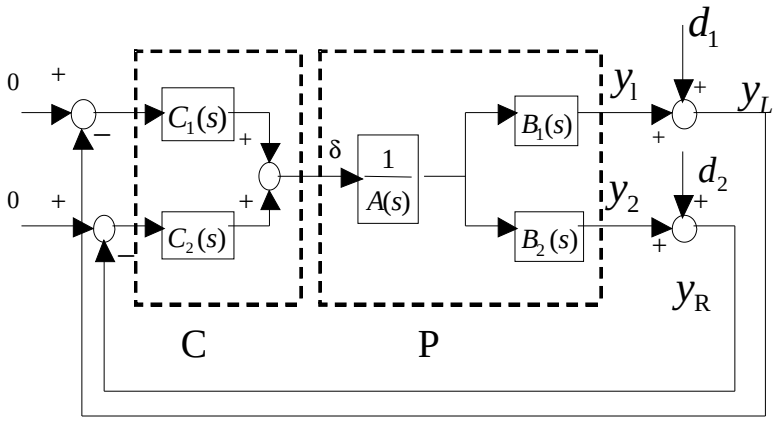

Figure 20: Control problem formulation

disturbance associated with the measurements from the rear set of magnetometers, y_R. As described in Section 2, vehicle lateral control performance with data from the rear magnetometers only is limited because of an unstable zero of the vehicle dynamics from δ to y_R. The benefit of using the information from the LIDAR sensor is that the dynamics from δ to y_L does not involve any unstable zero. In fact, the zero appears in the left-half side of the s-plane. However, the disadvantage of using the LIDAR sensor is that the disturbance, due to the unknown actual position and dynamics of the preceding vehicle, may affect the performance in terms of following the road centerline. Measurements from the rear magnetometers may be helpful in order to bring the vehicle back to the road centerline because they provide accurate measurements of the lateral deviation of the vehicle. The optimal way of combining these two sensor outputs can be achieved by careful controller design, based on the integrated closed loop system analysis. The control objective is to design a Two Input Single Output (TISO) controller such that no significant interactions occur in this closed loop control system within the system bandwidth, i.e., disturbances associated with one channel should have minimum effects on the other channel and vice versa. In particular, effect of d_1 on the rear magnetometer loop should remain small. Moreover, the controller should internally stabilize the control system and achieve optimal closed loop system performance.

5.2 Properties of Single Input, Two Output Feedback Systems

In Fig.19, let

$$P(s) = \begin{bmatrix} p_1(s) \\ p_2(s) \end{bmatrix} = \begin{bmatrix} \frac{B_1(s)}{A(s)} \\ \frac{B_2 s}{A(s)} \end{bmatrix} \tag{41}$$

$$C(s) = \begin{bmatrix} c_1(s) & c_2(s) \end{bmatrix} \tag{42}$$

The output sensitivity function is

$$S_o(s) = \Big(\ I + P(s)C(s) \ \Big)^{-1} \tag{43}$$

Let

$$S_o(s) = \begin{bmatrix} S_{11} & S_{12} \\ S_{21} & S_{22} \end{bmatrix} \tag{44}$$

Then the system outputs are written as,

$$\begin{bmatrix} y_L(s) \\ y_R(s) \end{bmatrix} = S_o \begin{bmatrix} d_1(s) \\ d_2(s) \end{bmatrix} = \begin{bmatrix} S_{11}d_1 + S_{12}d_2 \\ S_{21}d_1 + S_{22}d_2 \end{bmatrix} \tag{45}$$

The above equation implies that d_1 affects y_R, and d_2 affects y_L, only through the off-diagonal terms of S_o. Therefore, it is important to minimize the magnitude of these terms. In particular, S_{21} should remain small. The following theorem is summarized from the work done by Freudenberg and Middleton[2].

Theorem: For a fixed open loop gain $L = CP$, $max(|S_{21}|, |S_{12}|)$ is lower bounded, and the lower bound can be achieved iff

$$\frac{c_2(j\omega)}{c_1(j\omega)} = conj(\frac{p_2(j\omega)}{p_1(j\omega)}) \tag{46}$$

where $conj(x)$ represents the complex conjugate of x.

Proof: Let T_I be the complementary sensitivity function, i.e.

$$T_I = \frac{CP}{1 + CP} \tag{47}$$

Let

$$p_r = \frac{p_2}{p_1} \tag{48}$$

and

$$c_r = \frac{c_2}{c_1} \tag{49}$$

Then by applying the triangle inequality,

$$|S_{21}| \geq |T_I| \frac{|p_r|}{1 + |c_r p_r|} \tag{50}$$

and

$$|S_{12}| \geq |T_I| \frac{\frac{1}{|p_r|}}{1 + \frac{1}{|c_r p_r|}} \tag{51}$$

The equality holds if and only if $c_r p_r$ is real, i.e. $c_r = \alpha \bar{p}_r$, where α is a real number. It can be shown by comparing the two off-diagonal terms of S_o that $max(|S_{21}|, |S_{12}|)$ is lower bounded by $|T_I| \frac{|p_r|}{1+|p_r|^2}$, and the lower bound can be achieved if and only if α=1. End of proof.

More properties about SITO systems can be found in Freudenberg and Middleton[2], where the "alignment angle" is defined as

$$\phi(j\omega) = arccos(\frac{|C(j\omega)P(j\omega)|}{||C(j\omega)||.||P(j\omega)||}) \tag{52}$$

assuming that $P(j\omega) \neq 0$ and $C(j\omega) \neq 0$. The extent to which the two system outputs interact with each other can be quantified by using the alignment angle. It can be shown that $\phi(j\omega) = 0$ if and only if $\frac{c_2(j\omega)}{c_1(j\omega)} = conj(\frac{p_2(j\omega)}{p_1(j\omega)})$ Therefore, the lower bound as described in the above theorem is achieved if and only if the alignment angle is 0.

5.3 Proposed Controller Design Procedure

Based on the theorem described in the previous section, the proposed controller design procedure is as follows.

1. Determine a stable transfer function $W(s)$ which is the best approximation of $conj(\frac{p_1(j\omega)}{p_2(j\omega)})$, and define $c_1(s) = W(s)c_2(s)$. This will guarantee that the interactions between the system outputs as described in the previous section can be minimized.

2. Write $c_1(s)$ in terms of $c_2(s)$, absorb $W(s)$ into the plant, and convert the problem into a typical design problem for a SISO plant searching for c_2.

3. Choose suitable weighting functions, and apply conventional design techniques to find c_2, which minimizes the effects of the system disturbances on the regulated signals, such as lateral deviation and control input.

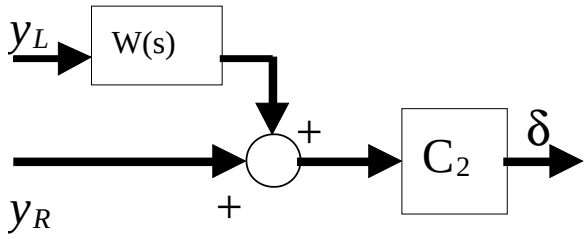

Figure 21: Formulation of controller

4. After c_2 is found, the controller C is formulated as shown in Fig.21.

Utilizing the parameter values in Table 1, $p_1(s)$ and $p_2(s)$ become

$$p_1(s) = \frac{216.1s^2 + 1160s + 4434}{s^4 + 8.861s^3 + 33.05s^2} \tag{53}$$

$$p_2(s) = \frac{-11s^2 - 92.22s + 4434}{s^4 + 8.861s^3 + 33.05s^2} \tag{54}$$

The frequency responses of $p_1(s)$ and $p_2(s)$ are shown in Fig.22 and 23. The weighting function is chosen to be

$$W(s) = \frac{-11s^2 - 92.22s + 4434}{216.1s^2 + 1160s + 4434} \tag{55}$$

which implies that $conj(\frac{p_2(j\omega)}{p_1(j\omega)})$ is approximated by $\frac{p_2(j\omega)}{p_1(j\omega)}$. This approximation is valid at low frequencies as shown in Fig.24. The controller c_2 designed in step 3 is

$$c_2(s) = \frac{\begin{array}{c} 0.1443s^8 + 16.56s^7 + 228.5s^6 + 1628s^5 + 6096s^4 \\ +12730s^3 + 5778s^2 + 1253s + 1.211 \end{array}}{\begin{array}{c} s^9 + 41.04s^8 + 791.8s^7 + 9463s^6 + 77490s^5 + 436000s^4 \\ +1395000s^3 + 2495000s^2 + 2518s + 0.02519 \end{array}} \tag{56}$$

The TISO controller can be constructed using c_2 and $W(s)$ as shown in step 4. The frequency responses of c_2 and c_1 are shown in Fig.25 and 26 respectively.

5.4 Simulation Results

Simulations have been conducted on a platoon of four vehicles. The lead vehicle was under normal magnetometer control with two sets of magnetometers, and the three

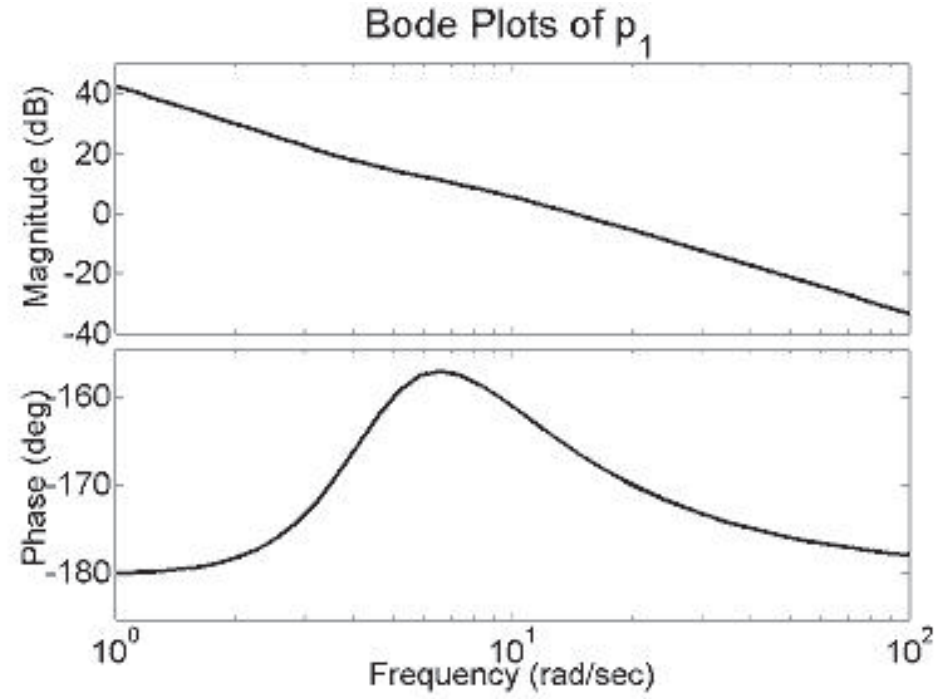

Figure 22: Bode plot of $p_1(s)$

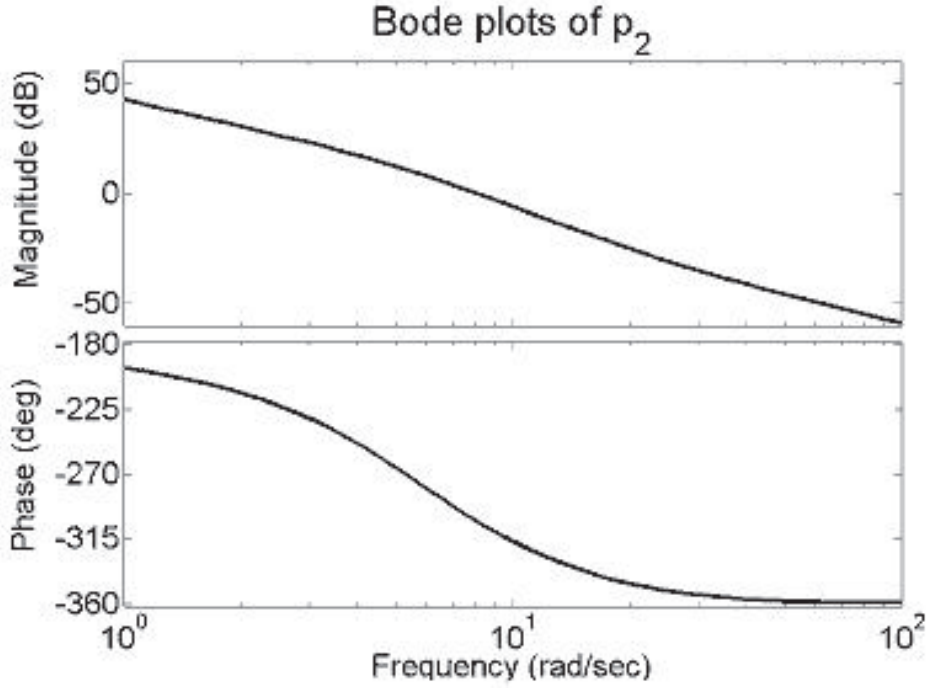

Figure 23: Bode plot of $p_2(s)$

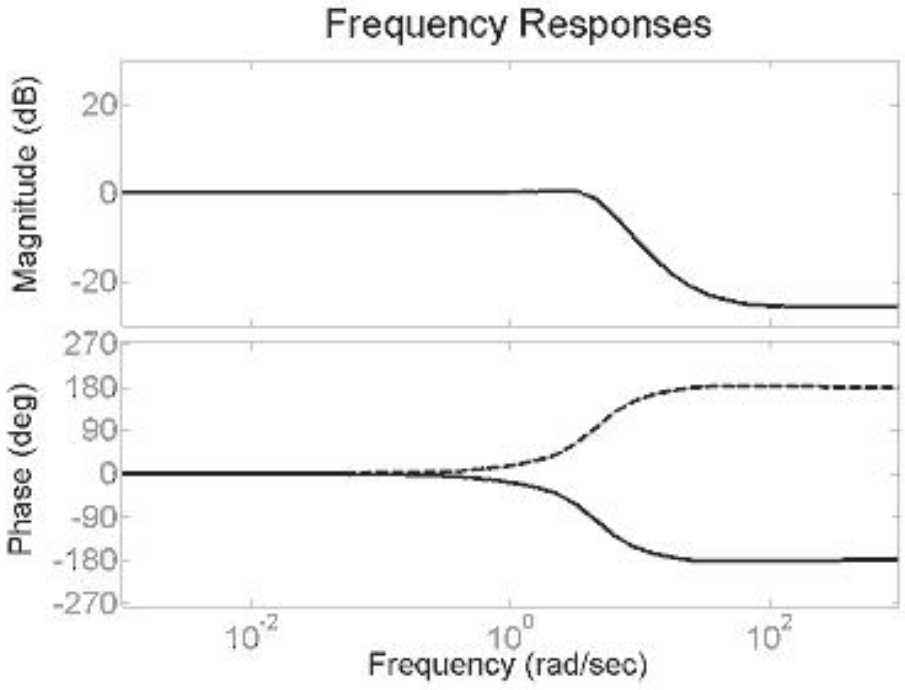

Figure 24: Frequency response of $W(j\omega)$ (solid) and $conj\{\frac{p_2(j\omega)}{p_1(j\omega)}\}$ (dashed)

following vehicles were under the control algorithm described in this section, i.e., each of them utilized measurements from the LIDAR sensor and rear magnetometers, pretending that the front magnetometers had failed. The longitudinal velocity used in the simulation increased from 20 m/s to 40 m/s and remained constant thereafter, as shown in Fig.27. Figure 28 shows the road curvature profile in the simulations. The simulated road consists of two curved sections, each having a constant road curvature of $\pm 1/800$ [1/m]. Figure 29 shows the simulation results. It is evident in the figure that the lateral deviation of each following vehicle is less than that of its preceding vehicle, although the three following vehicles were using exactly the same controller. The alignment angle is shown in Fig.30, in which it is clear that the controller and the plant are perfectly aligned within the closed loop bandwidth. It should be noted that the tracking performance would have been severely impaired if the feedback system had been obtained solely from the rear magnetometers.

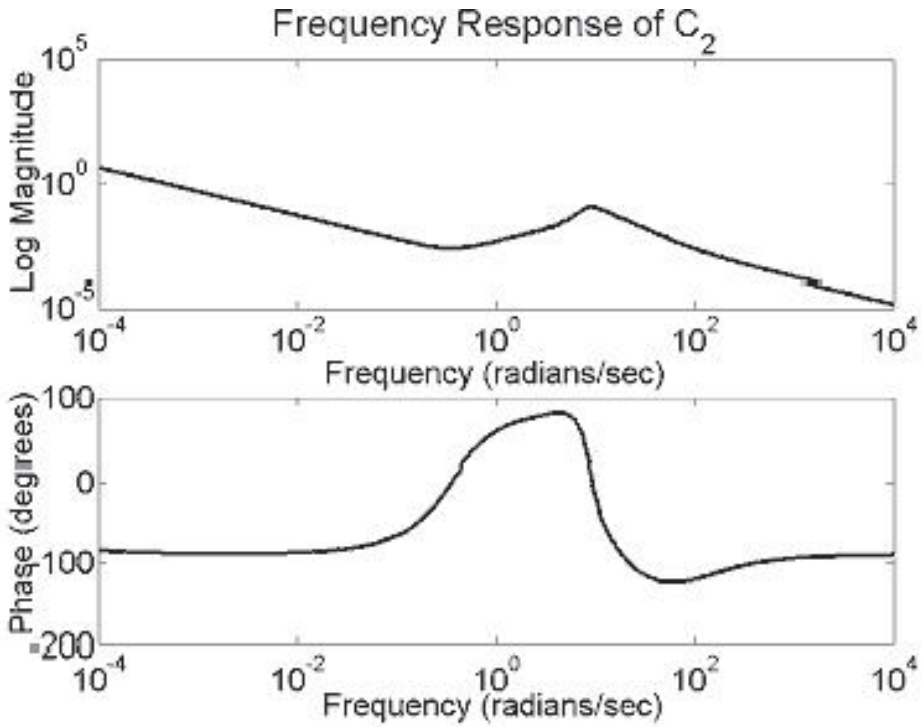

Figure 25: Frequency response of $c_2(s)$

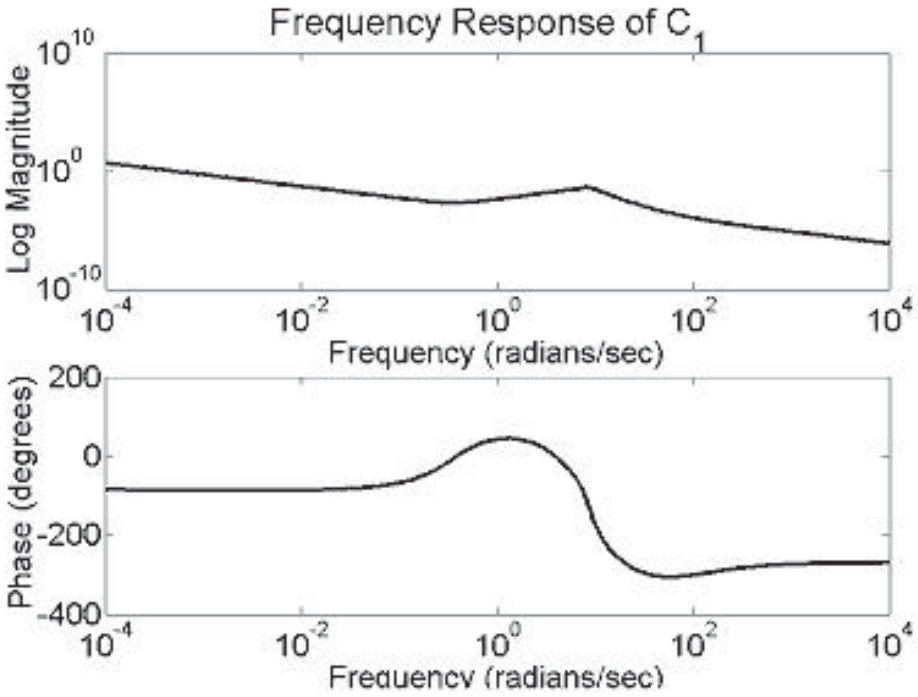

Figure 26: Frequency response of $c_1(s)$

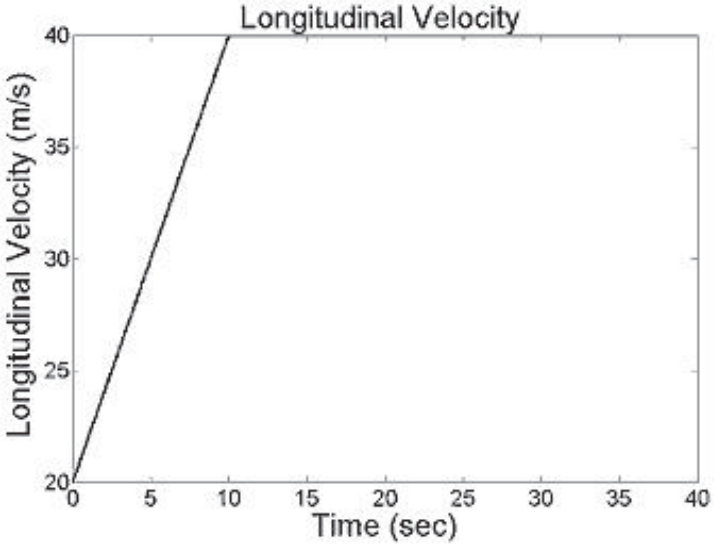

Figure 27: Longitudinal velocity profile

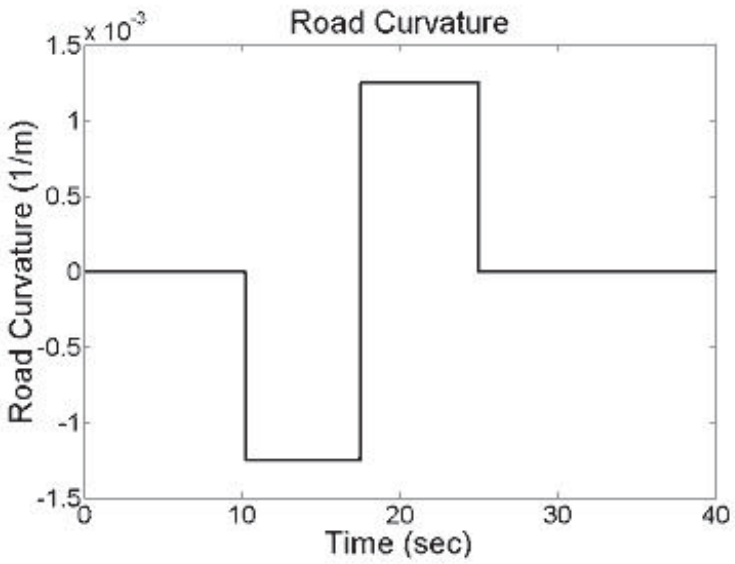

Figure 28: Road curvature profile

6 Conclusions

This report has described the development of degraded mode vehicle lateral control systems during the failures of magnetometers. Control algorithms have been developed for different magnetometer failure scenarios.

First, the design of an LTV controller for degraded mode vehicle lateral control under fault in rear magnetometers has been presented. The vehicle lateral dynamics with front magnetometer measurement as the output is sensitive to the changes of the longitudinal velocity; hence, to meet the performance requirements, an LTV controller is necessary. The LTV controller is designed based on feedback linearization with mismatched observer. The feedback linearization provides a simple and effective way of gain scheduling, and the mismatch observer prevent the weakly damped zeros of the vehicle lateral dynamics from being contained in the internal dynamics. The stability of the overall closed-loop system is examined and Quadratically Stability is achieved. Experiments have been conducted at Richmond Field Station, and the results demonstrate the effectiveness of the controller design.

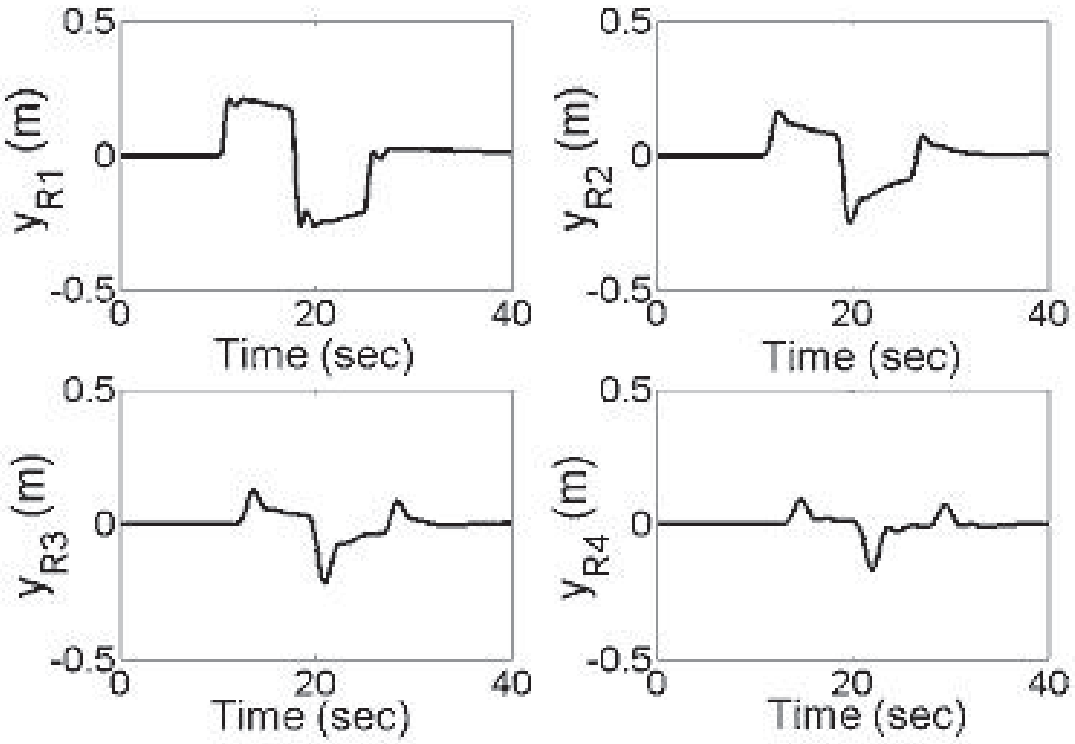

Figure 29: Lateral deviation of 4 vehicles in a platoon (y_{Ri} denotes the lateral deviation of the i th vehicle in the platoon measured by the rear magnetometers)

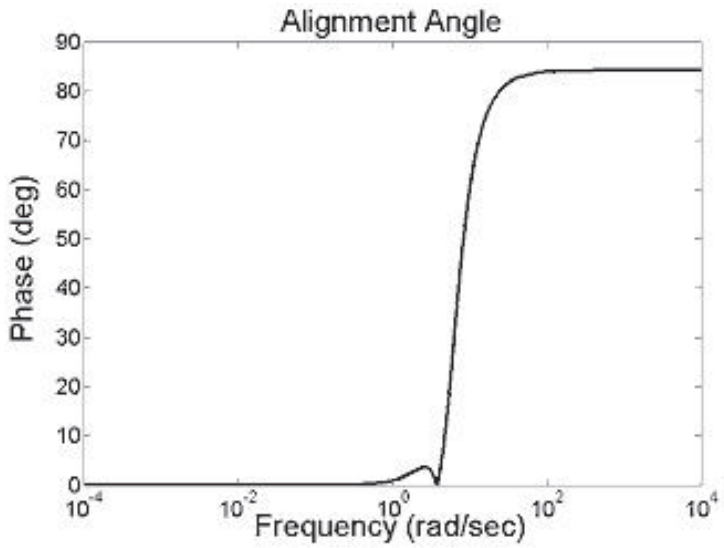

Figure 30: Alignment angle

Second, under the total failure of the magnetometers, a control algorithm based on the measurement of the relative position of the ego-vehicle with respect to its preceding vehicle by an on-board laser scanning radar sensor has been introduced. The effects of the spacing between the vehicles on the controller design is discussed. For safety reasons, the experiments are conducted at low speeds on a test track which represents more severe road curvature conditions than those on real highways, and the results prove the validity of the control system.

Third, when the front magnetometers fail, a back-up control system has been developed to combine the use of LIDAR with rear magnetometers. The controller design procedure is based on the minimization of the interactions of a single input, two output dynamic system for vehicle lateral control with combined use of the LIDAR sensor and the rear magnetometers. The design procedure guarantees good alignment of the plant and the controller within the closed loop bandwidth, ensuring no strong interactions in the closed loop system, i.e. the unknown actual position and dynamics of the preceding vehicle have little effects on the vehicle lane keeping performance. The simulation results verified that the proposed control scheme is a useful back-up

system in failure of front magnetometers.

Acknowledgement

This project is sponsored by California PATH (Partners of Advanced Transit and Highways) program. The contents of this report reflect the views of the authors who are responsible for the facts and the accuracy of the data presented herein. The contents do not necessarily reflect the official views or policies of the state of California. This report does not constitute a standard, specification, or regulation. We also acknowledge the technical contributions of Dr. H-S. Tan, D. Nelson, and other researchers at Richmond Field Station.

References

[1] Y. Bar-Shalom and T. E. Fortmann, "Tracking and Data Association", Academic Press, Inc., New York, NY, 1988

[2] J. Freudenberg and R. Middleton, "Properties of single input, two output feedback systems", *International Journal of Control*, 1999, Vol. 72, No. 16, 1446-1465

[3] J. Guldner, H-S Tan. and S. Patwardhan. (1997). "Study of Design Directions for Lateral Vehicle Control", *Proceedings of the 36th Conference on Decision and Control*, San Diego, California USA, December 1997.

[4] P. Hingwe, and M. Tomizuka, "Robust and gain scheduled H_∞ controllers for lateral guidance of passenger vehicles in AHS", *Proceedings of the ASME Dynamic Systems and Control Division*, DSC-Vol. 61, November 1997, pp. 707-713

[5] J. Huang, G. Lu, and M. Tomizuka, "Vehicle lateral control under fault in front and/or rear sensors", *California PATH Research Report*, UCB-ITS-PRR-2000-25

[6] S. Patwardhan, H-S Tan. and J. Guldner. (1997). "A general Framework for Automatic Steering Control: System Analysis", *Proceedings of the American Control Conference*, Albuquerque, New Mexico, June 1997.

[7] F. Wu, 1995, "Control of Linear Parameter Varying Systems", *PH. D. Dissertation*, Department of Mechanical Engineering, University of California, Berkeley.